ADVANCED MATERIALS
www.advmat.de

Fast Transfer of Triplet to Doublet Excitons from Organometallic Host to Organic Radical Semiconductors

Qinying Gu, Sebastian Gorgon, Alexander S. Romanov, Feng Li, Richard H. Friend, and Emrys W. Evans**

Spin triplet exciton formation sets limits on technologies using organic semiconductors that are confined to singlet-triplet photophysics. In contrast, excitations in the spin doublet manifold in organic radical semiconductors can show efficient luminescence. Here the dynamics of the spin allowed process of intermolecular energy transfer from triplet to doublet excitons are explored. A carbene-metal-amide (CMA-CF_3) is employed as a model triplet donor host, since following photoexcitation it undergoes extremely fast intersystem crossing to generate a population of triplet excitons within 4 ps. This enables a foundational study for tracking energy transfer from triplets to a model radical semiconductor, TTM-3PCz. Over 74% of all radical luminescence originates from the triplet channel in this system under photoexcitation. It is found that intermolecular triplet-to-doublet energy transfer can occur directly and rapidly, with 12% of triplet excitons transferring already on sub-ns timescales. This enhanced triplet harvesting mechanism is utilized in efficient near-infrared organic light-emitting diodes, which can be extended to other opto-electronic and -spintronic technologies by radical-based spin control in molecular semiconductors.

1. Introduction

Triplet excitons play a critical role in all technologies based on organic semiconductors, and effective spin management is required to achieve the desired optoelectronic properties. For closed-shell materials, organic light-emitting diodes (OLEDs) have well-known efficiency limits from the formation of 25% singlet and 75% triplet excitons with spin-allowed and -forbidden emission. The generation of dark triplet excitons that competes with charge extraction also hinders the performance in organic photovoltaics. The control of singlet and triplet states is critical in up- and down-conversion for photon management in imaging and increasing the spectral working range of devices such as photodetectors. In these technology areas, it is necessary to obtain light emission from triplet excitons, which can be achieved by a spin-flip (e.g., phosphorescence, thermally activated delayed fluorescence (TADF), triplet-triplet annihilation[1,2]) with performance limits set by singlet-triplet photophysics. Here we show the advantage of going beyond the singlet-triplet manifold in the presence of an open-shell organic radical with an all-doublet spin energy landscape. We present a foundational study of the triplet-doublet control mechanisms for harvesting energy from dark triplets with effective use as doublet excitons on organic radicals for luminescence.

To demonstrate the potential of triplet-doublet photophysics we designed a model system for studying direct spin-allowed energy transfer from triplet excitons generated within a closed-shell organic host to a doublet radical chromophore. We use a carbene-metal-amide (CMA-CF_3, **Figure 1a**) as a model host since following photoexcitation it undergoes extremely fast picosecond intersystem crossing (ISC) to generate a population of triplet excitons. This enables a direct measurement by optical spectroscopy, where the clock starts from picoseconds for tracking the subsequent energy transfer from triplets to TTM-3PCz (Figure 1a) radical doublet states for light emission. We show one application of this where our photophysical studies reflect the working mechanism in an efficient near-infrared OLED (705 nm, > 16% external quantum efficiency) for which the core process that needs to happen fast and efficiently is excitation transfer from triplets to doublets for electroluminescence. A rapid spin-allowed triplet-doublet transfer process overcomes the rate and performance

Q. Gu, S. Gorgon, R. H. Friend
Cavendish Laboratory
University of Cambridge
Cambridge CB3 0HE, UK
E-mail: rhf10@cam.ac.uk
Q. Gu
Shanghai Artificial Intelligence Laboratory
Shanghai 200232, P. R. China
A. S. Romanov
Department of Chemistry
University of Manchester
Oxford Rd., Manchester M13 9PL, UK
F. Li
State Key Laboratory of Supramolecular Structure and Materials
College of Chemistry
Jilin University
Qianjin Avenue 2699, Changchun 130012, P. R. China
E. W. Evans
Department of Chemistry
Swansea University
Singleton Park, Swansea SA2 8PP, UK
E-mail: emrys.evans@swansea.ac.uk

The ORCID identification number(s) for the author(s) of this article can be found under https://doi.org/10.1002/adma.202402790

DOI: 10.1002/adma.202402790

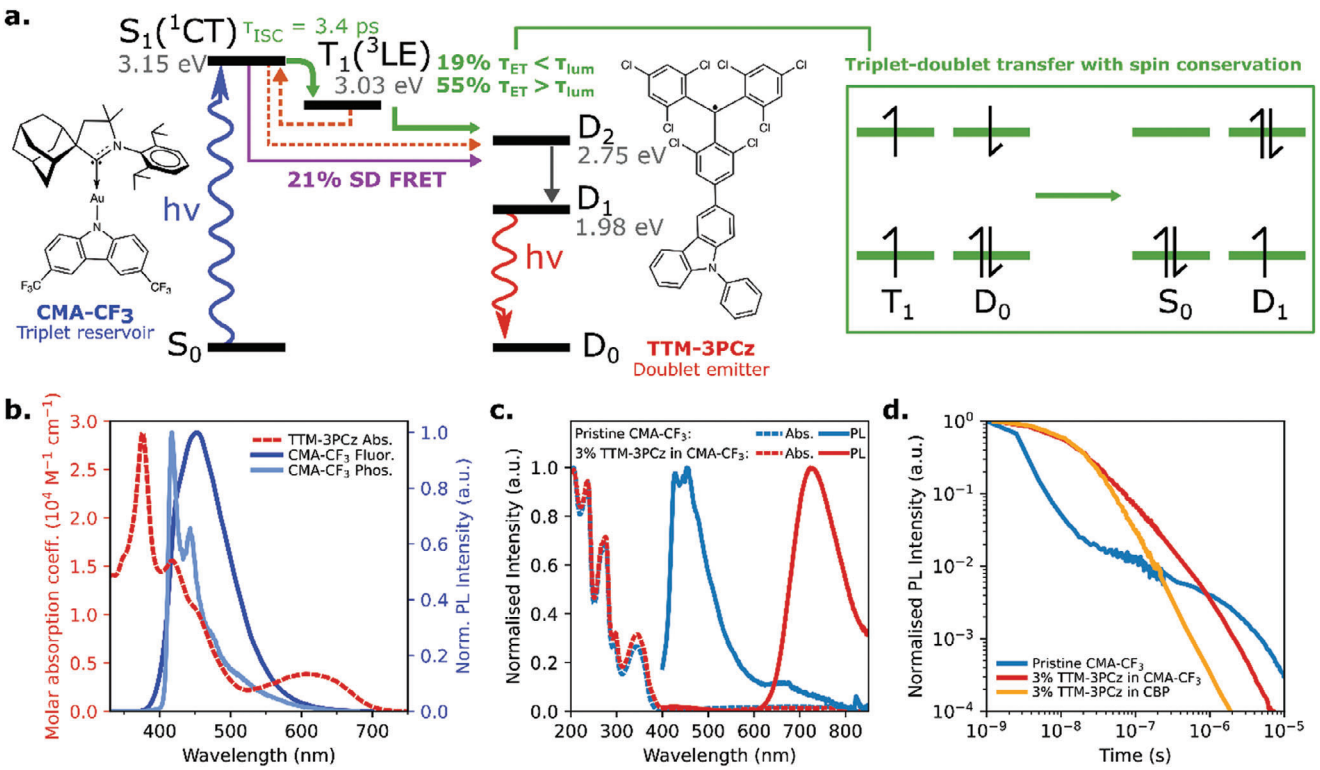

Figure 1. Model triplet-doublet energy transfer system with CMA-CF_3 and TTM-3PCz. a) Chemical structures of CMA-CF_3 and TTM-3PCz, and energy transfer mechanism in 3% TTM-3PCz in CMA-CF_3 blend with contributions to TTM-3PCz emission indicated as percentages. Example orbital configurations of triplet-doublet transfer with spin conservation are depicted. b) Molar absorption coefficient (red dashed line) of TTM-3PCz in THF, fluorescence (dark blue line) and phosphorescence (light blue line) spectra of CMA-CF_3 liquid toluene solution and frozen MeTHF respectively (excitation at 365 nm). Significant spectral overlap of the absorption and emission profiles enables energy transfer from S_1 and T_1 of CMA-CF_3 to TTM-3PCz. c) Absorption and steady-state PL spectra of 3% TTM-3PCz in CMA-CF_3 and pristine CMA-CF_3 films. CMA-CF_3 emission is completely quenched in the blend with only radical emission observed. d) Time-resolved PL of 3% TTM-3PCz (600–900 nm) in CMA-CF_3, 3% TTM-3PCz (600–900 nm) in 4,4′-*bis* (*N*-carbazolyl)−1,1′-biphenyl (CBP) and pristine CMA-CF_3 (400–600 nm) films. Delayed emission in 3% TTM-3PCz in CMA-CF_3 shows an activated energy transfer channel for radical emission that is faster than pristine CMA-CF_3, but slower than 3% TTM-3PCz in CBP.

limiting spin-flip step for light emission from triplet excitons in organic semiconductors.

Related singlet exciton energy transfer from a host TADF OLED system to a narrow band guest emitter (so-called hyperfluorescence) has been engineered to provide promising blue OLEDs.[3,4] The spin doublet emitter allows scope for direct energy transfer from the triplet excitons present in a host since this energy transfer process can be spin allowed. This was shown for a 4CzIPN (1,2,3,5-tetrakis(carbazol-9-yl)−4,6-dicyanobenzene) triplet harvesting host[5] and in the reverse process of doublet to triplet transfer[6] and in solution,[7] although these demonstrations were limited to microsecond timescales. Direct triplet energy transfer is attractive since it can speed up the emission rate by bypassing the slow reverse ISC step involving a spin-flip in TADF.

The theoretical treatment of energy transfer from closed-shell to open-shell (radical) materials was previously reported.[8] Singlet-doublet energy transfer can proceed via both Förster resonance energy transfer (FRET) and Dexter energy transfer (DET). Formally Coulomb-forbidden processes such as triplet-doublet energy transfer may become weakly allowed in the presence of spin-orbit coupling[9] that enables the FRET mechanism. Triplet-doublet DET is mediated via electron-exchange with spin conservation enabled by 2 of 6 encounter pairs that form an overall doublet multiplicity wavefunction.[5] A simplified scheme showing part of the orbital configurations involved in this mechanism is shown in Figure 1a.

The host CMA-CF_3 is chosen from a family of compounds with a molecular design of linear, two-coordinated coinage metal complexes where a metal atom bridges a cyclic (alkyl)(amino)carbene and carbazole as tunable electron π-acceptor and -donor components.[10–26] The generally observed picosecond ISC in carbene-metal-amides is driven by strong spin-orbit coupling derived from the coinage metal. Triplet states in carbene-metal-amides are long-lived up to microsecond timescales. By having tunable electronic and photophysical properties—whilst maintaining rapid ISC—as well as high thermal stability and insensitivity to aggregation quenching, this makes carbene-metal-amides the ideal host in model host-guest systems with organic radicals to study the mechanisms and fastest kinetics for triplet-doublet photophysics.[27]

The guest TTM-3PCz in our model system is a luminescent π-radical emitter that operates between a doublet spin energy manifold. The optical and doublet-spin properties of radicals enable efficient OLED demonstrations using a mechanism that avoids detrimental triplet exciton formation in device action.

Despite highly efficient OLED performance being reported for TTM-3PCz (Figure 1a) with 703 nm emission,[28] charge imbalance and accumulation at interface layers in this design are found to limit the device efficiency, stability and cause substantial reduction in performance at high current density ("roll-off").[29] Here the triplet-doublet photophysical mechanisms revealed from our studies of CMA-CF_3:TTM-3PCz enable enhanced performance for radical OLEDs. Triplets formed by direct electrical excitation of host sites, away from the radical, are harvested via energy transfer to the doublet emitter in an application where spin-flip limits can be removed in emission pathways starting from triplet excitons. We show that spin-allowed triplet-doublet energy transfer is efficient already on sub-nanosecond timescales, which is orders of magnitude faster than in triplet management technologies using singlet-triplet-limited photophysics.[1,2]

2. Results and Discussion

For energy transfer we require that the HOMO and SOMO levels of the TTM-3PCz energy acceptor lie between the HOMO and LUMO levels of the carbene-metal-amide host. Energy level values for TTM-3PCz and CMA-CF_3 were previously obtained from cyclic voltammetry in solution[12,28] and can be estimated in the solid state:[30] $HOMO_{TTM\text{-}3PCz} = -6.2$ eV; $SOMO_{TTM\text{-}3PCz(reduction)} = -3.5$ eV; $HOMO_{CMA\text{-}CF3} = -6.32$ eV; $LUMO_{CMA\text{-}CF3} = -2.58$ eV. We have tried several host candidates and found it was necessary to use two trifluoromethyl groups on the carbazole moiety in order to lower the HOMO energy of CMA-CF_3 below the TTM-3PCz HOMO to set up conditions for excited-state energy transfer to the radical component (Figure 1a). Other CMA candidates with cyano substitution and single trifluoromethyl have HOMO energies higher than the radical, and led to substantial host CMA emission in photoluminescence and electroluminescence from CMA:TTM-3PCz combinations as presented in Figure S1, Supporting Information. The favorable pairing of CMA-CF_3 and TTM-3PCz for energy transfer is demonstrated in Figure 1b where optical properties in tetrahydrofuran (THF) solvent show a significant spectral overlap of CMA-CF_3 delayed fluorescence (dark blue, measured at room temperature) and phosphorescence (light blue, measured at 77K) with the TTM-3PCz absorption profile (red). This supports energy conditions for transfer of excitations from singlet and triplet exciton states of CMA-CF_3 to TTM-3PCz radical. CMA-CF_3 shows structured deep blue emission ($\lambda_{max} = 425$ nm) in frozen 2-MeTHF at 77 K which is ascribed to local (i.e., ligand-centered) excited luminescence. The emission red-shifts in liquid toluene solution at room temperature and becomes broad and unstructured in this less-constrained environment, and is assigned to CT excited states[12] (Figure S2, Supporting Information for transient PL spectrum of solid-state CMA-CF_3). A broad and structured photoluminescence (PL) profile (Figure 1c) with major peaks at 425 and 470 nm is measured for the pristine CMA-CF_3 film, indicating that the emission in the solid state is mainly from the local-excited triplet state from the carbazole ligand, ^{3}LE(Cz), and is mixed with delayed luminescence of charge transfer CT character. Therefore, unlike the standard CMA1,[31] the emission of CMA-CF_3 films shows substantial phosphorescence contribution.[12] Thin-film PL of TTM-3PCz shows a strong CT character ascribed to electronic transitions from TTM-centered SOMO to 3PCz-HOMO in doublet fluorescence from D_1 (707 nm emission peak).[28]

To examine the effectiveness of CMA-CF_3 as a host for energy transfer, we measured the absorbance and steady-state PL of the pristine CMA-CF_3 film and 3% TTM-3PCz in CMA-CF_3 blend (Figure 1c) at film thickness of 80 nm. We excited the films at 355 nm, where CMA-CF_3 is strongly absorbing. The blend exhibits PL spectra near 715 nm due entirely to TTM-3PCz, and the CMA-CF_3 emission is quenched below the noise floor. Here TTM-3PCz emission is red-shifted by ≈10 nm compared to films in CBP, which is attributed to host polarity effects (Figure S3, Supporting Information). As direct TTM-3PCz photoexcitation is negligible, this shows that the radicals efficiently harvest CMA-CF_3 excitons by energy transfer for doublet emission.

2.1. Time-Resolved Spectroscopy

For tracking the dynamics of energy transfer, we performed time-resolved PL on ns-µs timescales. A 3% TTM-3PCz in CBP film was used as a reference since CBP has been shown to be a successful host in achieving efficient radical emission.[28] All samples were excited at 355 nm with fluences near 5 µJ cm^{-2}. As shown in Figure 1d, pristine CMA-CF_3 shows a multiexponential decay (400–600 nm averaged) with emission contributions from prompt and delayed fluorescence from ^{1}CT, as well as phosphorescence from ^{3}CT and ^{3}LE as previously reported.[12] However, on pairing CMA-CF_3 with TTM-3PCz, the 3% TTM:3PCz in CMA-CF_3 PL kinetics approaches that of the 3% TTM:3PCz in CBP blend (600–900 nm averaged). PL time slices exhibit only deep-red emission from the TTM-3PCz radical for the duration of the emission lifetime (Figure S4a, Supporting Information). The delayed component of the radical emission in the model blend is faster than delayed host emission in pristine CMA-CF_3, but slower than radical emission in 3% TTM-3PCz in CBP, suggesting that triplets are involved in energy transfer for TTM-3PCz in CMA-CF_3 blends.

To establish the earlier time kinetics, we performed transient absorption (TA) spectroscopy on ps-µs timescales. Following 355 nm excitation to achieve majority CMA-CF_3 host excitation, several overlapping photoinduced absorption (PIA) bands are present in the 3% TTM-3PCz in CMA-CF_3 blend, as shown in **Figure 2a**. To assign these excited-state features, we performed TA experiments on reference samples (Figure S5, Supporting Information). Photoexcitation of pristine CMA-CF_3 yields a broad PIA band centered at 660 nm that decays on ps timescales with the formation of a narrower band at 590 nm, which we assign to the CMA-CF_3 singlet (S_1) and triplet (T_1) excitons respectively. To establish the D_1 exciton profile of TTM-3PCz, we used samples of 3% TTM-3PCz in CBP and observed two PIAs centered at 620 nm and 1650 nm, matching our previous solution studies.[28,32]

As shown in Figure 2b, the bands identified in the control samples appear without any spectral shifts in the model 3% TTM-3PCz in CMA-CF_3 blend. Following photoexcitation into the CMA-CF_3 S_1 level, ISC occurs within the first few picoseconds to yield T_1 excitons. The TTM-3PCz D_1 level population grows continually until nanosecond timescales. We used a

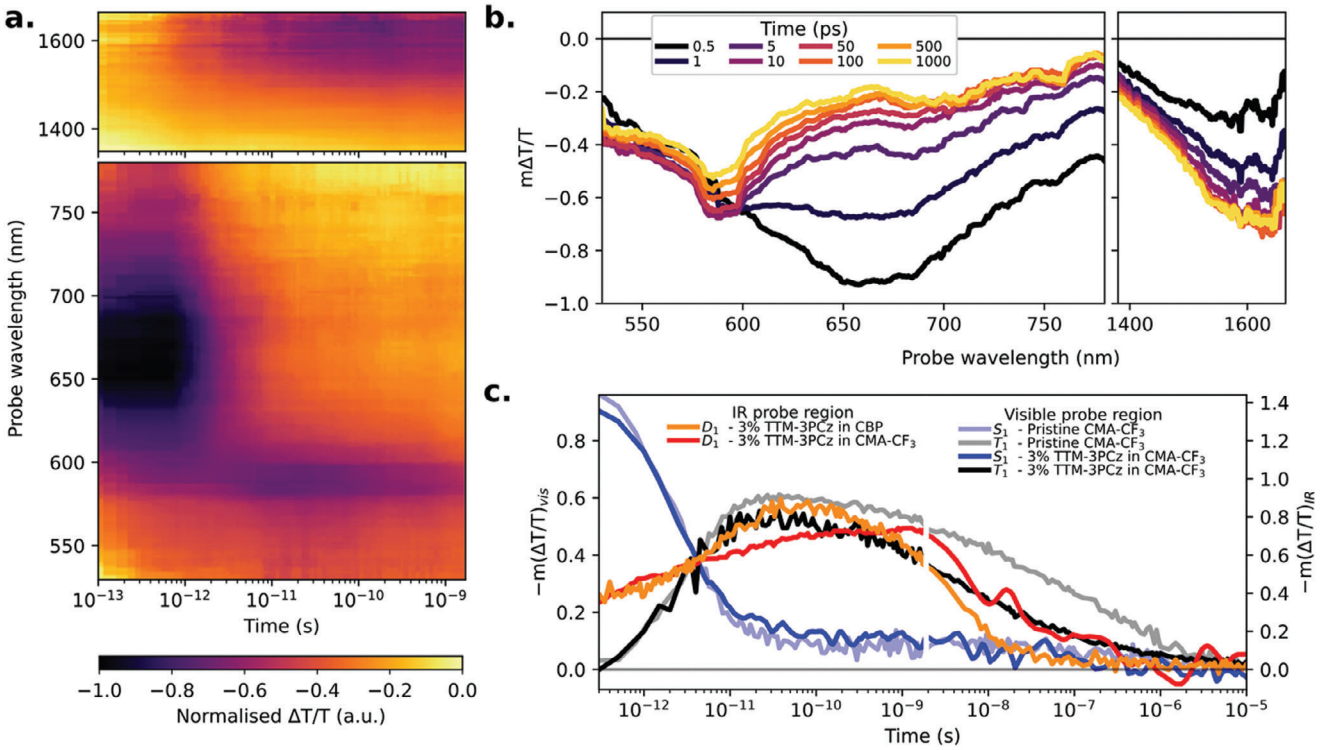

Figure 2. Excited state dynamics of TTM-3PCz and CMA-CF_3. a) Normalized transient absorption spectroscopy map of 3% TTM-3PCz in CMA-CF_3 following 355 nm excitation at fluence of 5.1 μJ cm^{-2}, with b) time slices of unnormalized spectra. PIA bands corresponding to CMA-CF_3 singlet S_1 and triplet T_1 excitons are centered at 660 and 590 nm respectively. TTM-3PCz doublet D_1 exciton PIAs are present at 1600 and 620 nm. c) Kinetics extracted from TA in 3% TTM-3PCz in CMA-CF_3 blend the reference 3% TTM-3PCz in CBP blend and pristine CMA-CF_3. Following fast ISC, the CMA-CF_3 T_1 decays faster in presence of TTM-3PCz. The D_1 population peaks around 1 ns and tracks the decay of the T_1 signal for the 3% TTM-3PCz in CMA-CF_3 blend, compared to peaking at 60 ps and displaying a faster decay for the 3% TTM-3PCz in CBP blend.

genetic algorithm to extract population-specific kinetic traces for the visible probe region (Supporting Information: Extracting population specific dynamics from TA, p. 6). The optimized species-associated spectra matched the bands seen in control samples (Figure S5a, Supporting Information) and allowed S_1 and T_1 kinetic traces to be extracted from the visible probe region data. We use the kinetics from the 1650 nm IR PIA to extract D_1 kinetic traces. These are shown in Figure 2c for the 3% TTM-3PCz in CMA-CF_3 blend of interest, and two control samples of pristine CMA-CF_3 and 3% TTM-3PCz in CBP blend.

The S_1 dynamics for CMA-CF_3 are unchanged in the presence of TTM-3PCz, as both pristine host and 3% blend show rapid ISC with a lifetime of 3.4 ps. This indicates that the introduction of radical dopants does not affect ISC dynamics within CMA-CF_3 excited states and confirms that triplet excitons are in excess of singlet excitons in the model blend already from 2.4 ± 0.3 ps.

The D_1 signal in 3% TTM-3PCz in CMA-CF_3 blend peaked at 1.1 ns, two orders of magnitude later than in the 3% TTM-3PCz in CBP control sample. Both samples show comparable direct radical absorption at the excitation wavelength and similar early time dynamics. Rapid energy transfer from CBP occurs exclusively via FRET from CBP singlets with a lifetime of 11.6 ps (Figure S5b, Supporting Information), which is similar to the S_1-D_1 FRET lifetime for the 3% TTM-3PCz in CMA-CF_3 blend calculated as 12 ps (Supporting Information: p. 5). Therefore, in the TTM-3PCz in CMA-CF_3 blend, singlet to doublet FRET is largely outcompeted by rapid ISC, and occurs with a quantum yield of ≈21%. Since singlet-doublet FRET is not the dominant energy transfer pathway, we can focus on the triplet-doublet energy transfer (TDET) channel contributions to the blend photophysics.

The T_1 population peaked at 38 ps in pristine CMA-CF_3, but at 24 ps in the 3% TTM-3PCz in CMA-CF_3 blend. It decayed faster with increasing TTM-3PCz loading, with its fastest decay lifetime decreasing from 200 ns in pristine CMA-CF_3, to 70 ns in 3%, and further to 30 ns in 5% TTM-3PCz in CMA-CF_3 blends (Figures S6 and S7, Supporting Information). This suggests that CMA-CF_3 triplet excitons undergo energy transfer to TTM-3PCz sites on picosecond to nanosecond timescales. We consider that the slower transfer rates are limited by the speed of triplet exciton hopping between CMA-CF_3 sites until they are in spatial range of a TTM-3PCz molecule, and forming an encounter pair in a spin configuration that allows energy transfer.[33] To estimate the fraction of TDET by a given time we compare the loss of T_1 population seen in TA of the blend versus pristine CMA-CF_3. We observe that 23% of triplet excitons transfer within one radical radiative lifetime (21.2 ns[28]) and 12% of triplet excitons transfer within 1 nanosecond.

The TA results show that triplet excitons play the dominant role in energy transfer. To gain insight into the mechanism of TDET we performed temperature-dependent time-resolved PL spectroscopy. At room temperature, analysis of the integrated PL

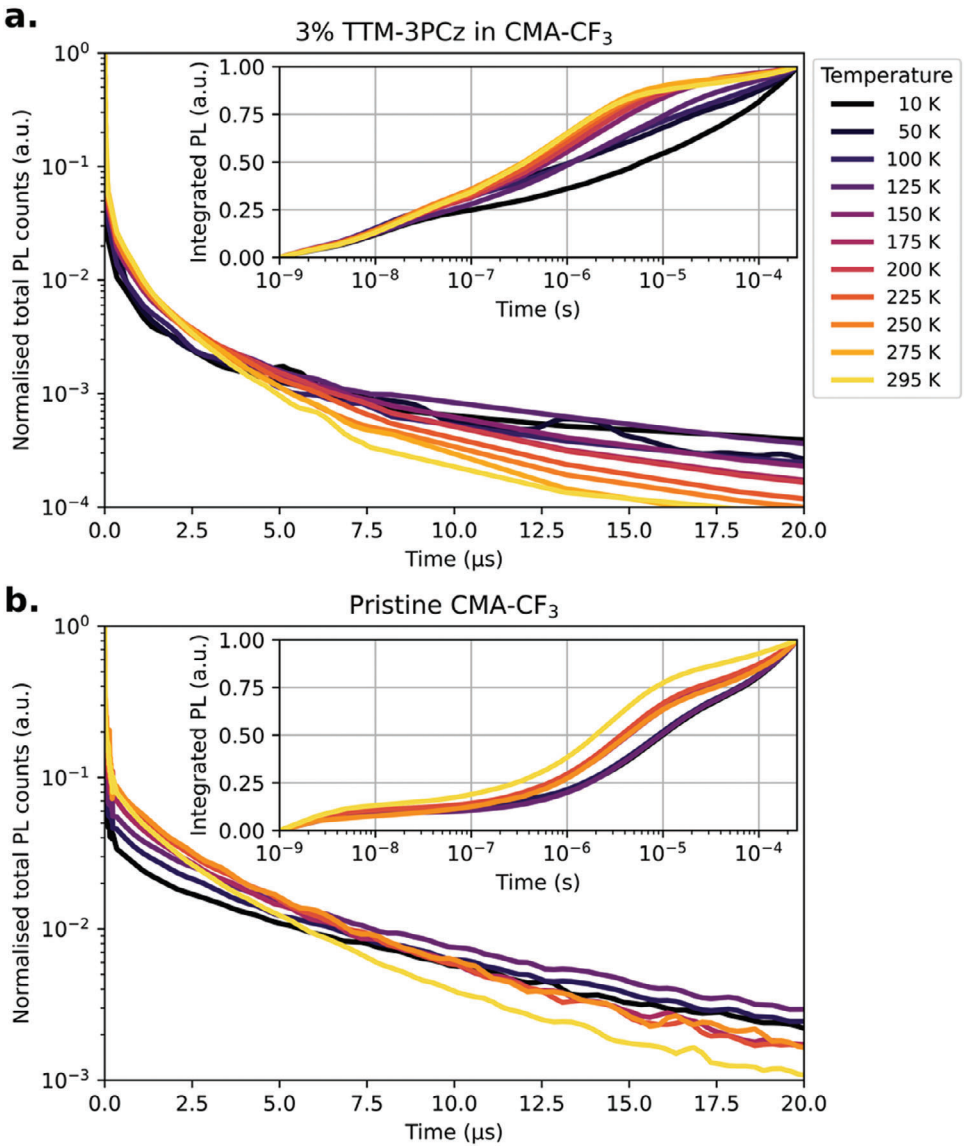

Figure 3. Temperature-dependent emission dynamics of TTM-3PCz and CMA-CF_3. Temperature-dependence on the time-resolved PL kinetics of a) 3% TTM-3PCz in CMA-CF_3 and b) pristine CMA-CF_3 films following 355 nm excitation. Insets show integrated PL. Lowering of activation energy compared to pristine host shows that hyperfluorescence is not responsible for delayed emission in 3% TTM-3PCz in CMA-CF_3 blend.

(**Figure** 3a, inset) reveals that 24% of all emission in the blend occurs within one radical radiative lifetime. This matches the TA results and suggests the majority of triplet excitons transfer at later times. From the fraction of delayed radical emission, we estimate this fraction at 55%. Upon cooling, the delayed emission is significantly slower in both the 3% TTM-3PCz in CMA-CF_3 blend (Figure 3a) and pristine CMA-CF_3 (Figure 3b). TTM-3PCz in CMA-CF_3 showed no changes to the emission spectra upon cooling. We used Arrhenius analysis of k_{RISC} (rate of reverse ISC, RISC) against the inverse of temperature to estimate the activation energies (E_a), following methodology for delayed fluorescence systems (Figure S4, Supporting Information). For pristine CMA-CF_3, the activation energy was found to be 70 ± 1 meV. The key temperature-activated process in pristine CMA-CF_3 is the RISC from triplet to singlet excitons, and this value shows good agreement with the calculated ΔE_{ST} for CMA-CF_3 (120 meV) from fluorescence and phosphorescence spectra. This large activation energy makes RISC relatively slow. However, for the 3% TTM-3PCz in CMA-CF_3 blend the activation energy calculated from the Arrhenius equation was found to be $E_a = 24 \pm 8$ meV. This shows the delayed component of radical emission is not due to thermal excitation of triplet to singlet excitons followed by singlet-doublet energy transfer, hyperfluorescence, since this would require the same activation energy.[27] Therefore, as the activation energy is lower in blends compared to pristine CMA-CF_3, RISC to the singlet level is not mediating energy transfer from triplets to TTM-3PCz doublets. We consider the lower activation energy of the TTM-3PCz:CMA-CF_3 blend reflects the emergence of triplet-doublet energy transfer pathways for delayed emission in this system.

2.2. Discussion of Energy Transfer Mechanism

Our time-resolved spectroscopy results demonstrate that T_1 triplet excitons accumulate rapidly following photoexcitation of CMA-CF_3 and this provides a model system to study the subsequent energy transfer from this triplet population. Due to the rapid ISC, SD FRET is not a significant channel in this blend. We observe energy transfer directly from triplets to form doublet excitons in TTM-3PCz, with some TDET occurring already on picosecond timescales. Two of the main energy transfer mechanisms in organic systems are FRET and DET.[33–43] FRET occurs through a long-range dipole-dipole electromagnetic interaction and its efficiency is dependent on the spectral overlap integral between the emission profile of the host (CMA-CF_3) and the absorption of the dopant (TTM-3PCz).[40,44] The triplets in CMA-CF_3 can also undergo FRET because CMA-CF_3 is phosphorescent. Although "pure" triplets have no oscillator strength and are generally not active in FRET, enhanced spin-orbit coupling derived from the metal center makes the CMA-CF_3 triplets emissive, and they can be radiatively dipole-coupled to radicals for energy transfer. As shown in Figure 1b, the absorption of TTM-3PCz overlaps well with the phosphorescence spectrum of CMA-CF_3 indicating the triplet to doublet energy transfer via Förster type is possible. FRET can be therefore used to harvest energy from both singlet and triplet CMA-CF_3 excitons. Energy transfer is also achievable via DET in an electron-exchange mechanism, whose efficiency depends on the overlap of molecular orbitals on adjacent molecule.

As the doublet population dynamics show a stretched rise and decay, and DET requires close molecular proximity, we expect the picosecond-DET to occur from excited CMA-CF_3 sites directly adjacent to a TTM-3PCz, We consider the rate of nanosecond-DET to be limited by triplet diffusion (cf. Figure S7, Supporting Information) that underpins the activation energy of delayed PL.

Additionally, part of the nanosecond energy transfer may originate in a FRET mechanism from distant T_1 excitons that have not encountered a TTM-3PCz site directly. As the phosphorescence of CMA-CF_3 and the absorption of TTM-3PCz overlap around 450 nm (Figure 1b), which corresponds to the energy of the second doublet excited state (≈2.75 eV) of TTM-3PCz, direct FRET can take place from T_1 to D_2. D_2 excitons can undergo rapid internal conversion to D_1, and then fluorescence to the D_0 ground state.

In summary, we identify two direct triplet-doublet energy transfer routes: the dominant fast channel occurring on sub-20 ns times which accounts for 19% of emitted photons, made up of temperature independent Dexter transfer from T_1 to D_1 with a possible contribution of TD FRET for nanosecond timescales. This is followed by slower, temperature-activated triplet diffusion within the CMA-CF_3 host matrix where triplets can encounter a radical site in range and in an allowed spin configuration for TDET, leading to 55% of emitted photons. The smaller activation energy for delayed emission in the blend compared to the pristine host indicates that the excitation transfer process is direct and not mediated by "hyperfluorescence." The remaining emitted photons originate from excitons transferred via FRET from the singlet level (21%) and weak direct TTM-3PCz absorption (5%). Our study pushes the boundary of emission times in organic semiconductors limited by delayed fluorescence or phosphorescence from triplet excitons.[45] We show triplet-doublet transfer can be an efficient and fast mechanism for harvesting emissive excitations in organic semiconductors using a luminescent radical energy sink where doublet excitons are degenerate or have lower energy than triplet excitons in a system.

2.3. Device Performance and Physics

Our radical-based method for efficient light emission that originates from triplet excitons (Figure 1a) can advance performance and unlock possibilities for spin control in optoelectronics, optospintronics, and photon management technologies from organic semiconductors. Here we target demonstrations in OLEDs to show one application that emerges from using triplet-doublet photophysics. Several device structures were prepared by vacuum thermal deposition and the following architecture was found to give the best performance: indium tin oxide (ITO)/molybdenum trioxide (MoO_3) (5 nm)/1,1-*bis*[(di-4-tolylamino)phenyl]cyclohexane (TAPC) (40 nm)/emissive layer (EML) (30 nm)/4,6-*bis*(3,5-di-3-pyridylphenyl)−2-methylpyrimidine (B3PYMPM) (60 nm)/lithium fluoride (LiF) (0.8 nm)/aluminum (Al) (100 nm) (**Figure 4a**). The optimized device shows near infrared (NIR) electroluminescence (EL, λ_{max} = 705 nm) with a maximum external quantum efficiency (EQE) of 16.0%, which ranks among the highest EQE values for NIR OLEDs employing purely organic emitters.[46,47] The low turn-on voltage (3.8 V) and high achievable radiance are also competitive compared to previously reported radical-based OLEDs.[28,48] The emission of the device is only from TTM-3PCz across the applied voltage from 5 to 10 V (Figure 4d), with efficient quenching of the CMA-CF_3 EL. We optimized the OLED device stack in terms of the selection and thickness control of EML and the electron transport layer (ETL) to achieve negligible current leakage and therefore good charge balance (see Figures S8–S11, Supporting Information) for current density–voltage and radiance–voltage characteristics of other device stacks). The EML composition of 3% TTM-3PCz in CMA-CF_3 balances having efficient CMA-CF3 to TTM-3PCz energy transfer and reducing TTM-3PCz concentration quenching effects (Table S2, Supporting Information) that lead to lower PLQE and EQE. All devices show high EQEs at low current density together with good reproducibility. Generally, improved device performance (higher EQE, higher radiance, lower efficiency roll-off) was observed for TTM-3PCz:CMA-CF3 OLEDs compared to TTM-3PCz:CBP reference devices (Figure S12, Supporting Information).

The main exciton formation mechanism in 3% TTM-3PCz in CMA-CF_3 OLEDs is considered to be the energy transfer mechanism from excited CMA-CF_3 as studied in thin film photophysics. We also replaced the B3PYMPM for 2,2′,2′′-(1,3,5-benzinetriyl)-tris(1-phenyl-1-H-benzimidazole) (TPBi): 1,4-*bis*(triphenylsilyl)benzene (UGH2) (9:1 wt%, 10 nm) and TPBi (60 nm) where TPBi and UGH2 are ETL and hole blocking layers, respectively. Here the LUMO energies are closer to that of CMA-CF_3 so that it is more preferentially excited over TTM-3PCz when using the TPBi:UGH2 transport layer compared to B3PYMPM.[12,31] This device shows 14.9% maximum

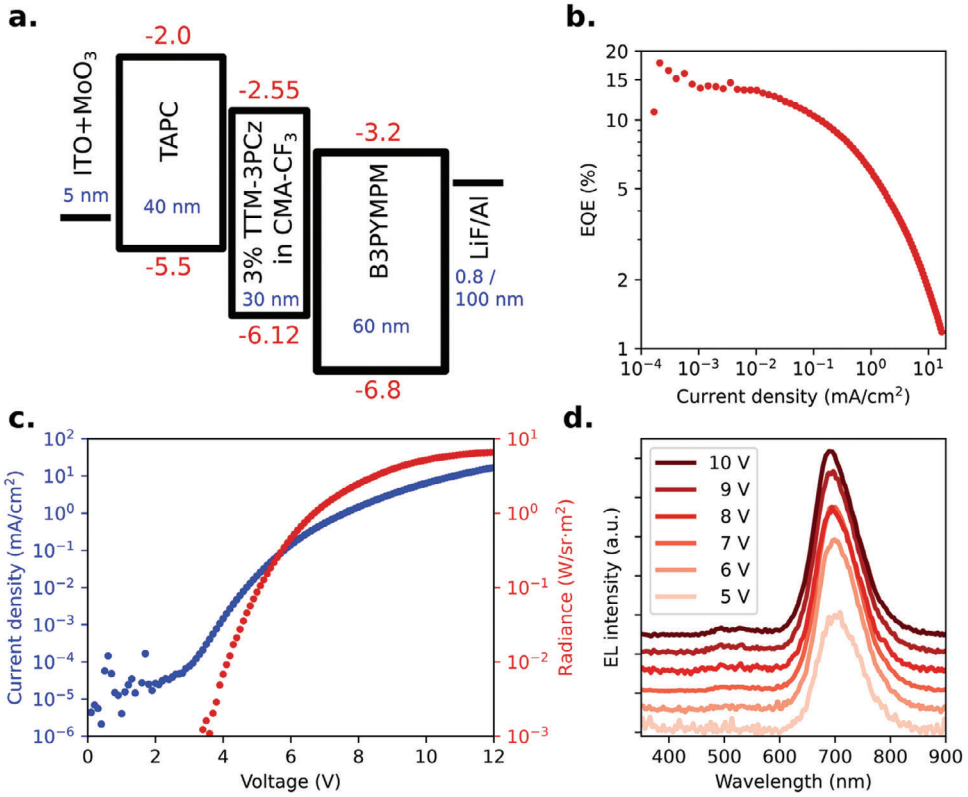

Figure 4. OLED characteristics of TTM-3PCz and CMA-CF_3. a) Optimized device structure for 3% TTM-3PCz: CMA-CF_3 OLED. b) EQE versus current density with a maximum EQE of 16.0%. c) Current density versus voltage (blue) and radiance versus voltage (red) of the 3% TTM-3PCz: CMA-CF_3 device. d) EL spectra of the champion device from 5 to 10 V indicating 3% TTM-3PCz: CMA-CF_3 device is from TTM-3PCz.

EQE and no residual emission from CMA-CF_3 can be seen (Figure S12, Supporting Information), consistent with our energy transfer mechanism.

Additionally, magneto-electroluminescence (MEL) studies were conducted to obtain further mechanism insights from the carrier spin dynamics in working OLEDs.[49–52] In the reference 4,4′-*bis*(*N*-carbazolyl)−1,1′-biphenyl (CBP)-based OLED (Figure S13, Supporting Information), we found negligible MEL effects, which are consistent with previous observations in radical OLEDs with direct doublet electrical excitation.[50] A positive MEL was observed in the 3% TTM-3PCz in CMA-CF_3 device. The magnetosensitivity is attributed to Zeeman splitting[53,54] of triplet exciton sublevels, with positive MEL effects from increased triplet CMA-CF_3 exciton populations in the presence of magnetic field, and therefore an enhanced triplet-to-doublet energy transfer.[55]

Device stability is a key property that must be realized for the practical use of radical OLEDs. Compared to 3% TTM-3PCz in CBP devices, where lifetimes are limited to minutes timescales, our device using the energy transfer mechanism has an order of magnitude of improvement in lifetime to around 1 h at the same current density without device encapsulation (Figure S14, Supporting Information for the device stability comparison). We attribute the device improvement to the ability of CMA-CF_3 to promote electrical excitation away from radical sites in this design, with doublet excitons for infrared emission formed by efficient energy transfer from CMA-CF_3 to TTM-3PCz as demonstrated in our photophysics studies.

There is an even larger improvement in device stability compared to the pristine CMA-CF_3. Degradation of carbene-metal-amides is considered to be due to the presence of excitons rather than charges.[56] This is particularly severe for the CMA-CF_3 material used here, for which device lifetimes are only a few seconds (Figure S14, Supporting Information). However, in our device design, efficient energy transfer quickly depopulates the high-energy triplet excitons from CMA-CF_3, avoiding the degradation caused by high-energy states. Our successful demonstration of a radical energy transfer system in optoelectronics shows the potential of higher performance limits and novel technology platforms from singlet-triplet-doublet photophysics.

3. Conclusions

In summary, we explored the rate limits of spin-allowed triplet to doublet energy transfer and demonstrated that the process can occur on sub-nanosecond timescales. These foundational studies of a triplet-doublet energy manifold were conducted in a model system using triplet excitons from CMA-CF_3 and doublet-spin radicals from TTM-3PCz. Due to the few-picosecond ISC in CMA-CF_3, which leads to rapid generation of triplet excitons in high yield by optical excitation, the triplet-doublet transfer mechanisms can be tracked in spectroscopic studies of the model system as enabled here by 74% of radical emission taking this channel. We show that some excitons transfer from CMA-CF_3 T_1 to TTM-3PCz D_1 states within hundreds of picoseconds and

attribute this to an efficient triplet-doublet process, showing that triplet management mechanisms for emission can be accelerated by orders of magnitude compared to spin-flip schemes in standard singlet-triplet photophysics. A demonstration of OLEDs using this system translated the triplet-doublet mechanism enabling emission from triplet excitons that otherwise limit the device performance. High EQEs of up to 16.0% were achieved in TTM-3PCz:CMA-CF_3 devices with near infrared 705 nm electroluminescence derived from triplet-doublet energy transfer. The mechanism is applicable to all technology platforms using organic semiconductors in applications ranging from imaging to communications, to where radical spin control overcomes performance limits in opto-electronics and -spintronics, and the possibilities created from enhanced luminescence in molecular materials.

4. Experimental Section

Materials: TTM-3PCz and CMA-CF_3 were synthesized as previously reported.[12,28] TAPC, B3PYMPM, CBP of sublimed grade, and other OLED materials were obtained from Ossila and Lumtec.

Photophysics: Optical spectroscopy measurements (time-resolved PL and transient absorption, TA) were conducted on home-built setups powered by a Ti:Sapphire amplifier (Spectra Physics Solstice Ace, 100 fs pulses at 800 nm, 7 W at 1 kHz). Time-resolved PL studies were performed with an Andor spectrometer setup using a spectrograph and electrically gated intensified CCD camera (Andor SR303i; Andor iStar). Sample photoexcitation with 355 nm pump pulses was provided by frequency doubling of the output of a home-built narrowband visible Noncollinear Optical Parametric Amplifier (NOPA) pumped by 1 W of the Ti:Sapphire output for time-resolved PL experiments. 355 nm pump pulses for the short-time (<2 ns) TA studies were prepared in a similar way. The third harmonic of an electronically triggered Q-switched Nd:YVO4 (1 ns pump length, Advanced Optical Technologies Ltd AOT-YVO-25QSPX) laser was used as the source of 355 nm pump pulses for the long-time (> 1 ns) TA studies. Broadband NOPAs were used to generate probe pulses for TA in the visible (510–780 nm) and infrared (1250–1650 nm) wavelength ranges. NOPA probe pulses were divided into two identical beams by a 50/50 beamsplitter, allowing the use of a reference beam for improved signal:noise. Custom-built Si (Hamamatsu S8381-1024Q) and InGaAs (Hamamatsu G11608-512DA) dual-line arrays from Stresing Entwicklungsbüro were used to detect probe and reference pulses.

Device Fabrication and Characterization: An Angstrom Engineering EvoVac 700 system was used to fabricate organic semiconductor films and devices by vacuum deposition (10^{-7} torr). Current density, voltage, electroluminescence characteristics, and device lifetimes were obtained from a Keithley 2400 sourcemeter, Keithley 2000 multimeter, and calibrated silicon photodiode in a home-built setup. Magneto-electroluminescent (EL) measurements were performed with Andor spectrometer (Shamrock 303i and iDus camera) to monitor the modulation of EL in presence of a magnetic field applied by GMW 3470 electromagnet.

Supporting Information

Supporting Information is available from the Wiley Online Library or from the author.

Acknowledgements

Q.G. is grateful to the Cambridge Trust and China Scholarship Council (grant no. 201808060075) for the financial support. Q.G. additionally acknowledges funding from the National Key R&D Program of China (no. 2022ZD016101). S.G. acknowledges funding from the EPSRC Centre for Doctoral Training in Integrated Functional Nano (grant EP/S022953/1) and Christ's College, Cambridge. F.L. is grateful for financial support from the National Natural Science Foundation of China (grant no. 51925303) and the programme "JLUSTIRT" (grant no. 2019TD-33). F.L. is an academic visitor at the Cavendish Laboratory, Cambridge, and is supported by the Talents Cultivation Programme (Jilin University, China). R.H.F. acknowledges support from the Simons Foundation (grant no. 601946) and the EPSRC (EP/M005143/1). E.W.E. is grateful to the Royal Society for a university research fellowship (grant no. URF\R1\201300) and EPSRC (EP/W018519/1) for funding. This project received funding from the ERC under the European Union's Horizon 2020 research and innovation programme (grant agreement number 101020167). A.S.R. acknowledges the support from the Royal Society (grant no. URF\R1\180288, RGF\EA\181008, URF\R\231014), EPSRC (grant code EP/K039547/1).

Conflict of Interest

The authors declare no conflict of interest.

Author Contributions

Q.G. and S.G. contributed equally to this work. Q.G. fabricated thin-films and optimized OLED devices, which were characterized by photoluminescence, device performance measurements, and magnetic field studies. S.G. carried out the transient absorption measurements, data analysis, and model calculation. Q.G. and S.G. performed the temperature-dependent time-resolved PL. F.L. and A.S.R. synthesized and provided the materials. R.H.F. and E.W.E. conceived the project and supervised the work. All authors contributed to the result analysis and manuscript writing.

Data Availability Statement

The data that support the findings of this study are openly available in University of Cambridge at https://doi.org/10.17863/CAM.109299.

Keywords

doublet emission, exciton management, organic light-emitting diodes, photophysics, radical materials

Received: February 23, 2024
Revised: May 9, 2024
Published online:

[1] R. Pode, *Renewable Sustainable Energy Rev.* **2020**, *133*, 110043.
[2] S.-J. Zou, Y. Shen, F.-M. Xie, J.-D. Chen, Y.-Q. Li, J.-X. Tang, *Mater. Chem. Front.* **2020**, *4*, 788.
[3] C.-Y. Chan, M. Tanaka, Y.-T. Lee, Y.-W. Wong, H. Nakanotani, T. Hatakeyama, C. Adachi, *Nat. Photonics* **2021**, *15*, 203.
[4] S. O. Jeon, K. H. Lee, J. S. Kim, S.-G. Ihn, Y. S. Chung, J. W. Kim, H. Lee, S. Kim, H. Choi, J. Y. Lee, *Nat. Photonics* **2021**, *15*, 208.
[5] F. Li, A. J. Gillett, Q. Gu, J. Ding, Z. Chen, T. J. Hele, W. K. Myers, R. H. Friend, E. W. Evans, *Nat. Commun.* **2022**, *13*, 2744.
[6] J. Han, Y. Jiang, A. Obolda, P. Duan, F. Li, M. Liu, *J. Phys. Chem. Lett.* **2017**, *8*, 5865.
[7] Z. Chen, G. Liang, K. Wu, *J. Mater. Chem. C* **2022**, *10*, 4697.
[8] K. R. Naqvi, *J. Phys. Chem.* **1981**, *85*, 2303.
[9] R. E. Kellogg, R. G. Bennett, *J. Chem. Phys.* **1964**, *41*, 3042.

[10] J. Eng, S. Thompson, H. Goodwin, D. Credgington, T. J. Penfold, *Phys. Chem. Chem. Phys.* **2020**, *22*, 4659.
[11] A. S. Romanov, F. Chotard, J. Rashid, M. Bochmann, *Dalton Trans.* **2019**, *48*, 15445.
[12] P. J. Conaghan, C. S. Matthews, F. Chotard, S. T. Jones, N. C. Greenham, M. Bochmann, D. Credgington, A. S. Romanov, *Nat. Commun.* **2020**, *11*, 1758.
[13] M. Melaimi, R. Jazzar, M. Soleilhavoup, G. Bertrand, *Angew. Chem., Int. Ed.* **2017**, *56*, 10046.
[14] S. Thompson, J. Eng, T. Penfold, *J. Chem. Phys.* **2018**, *149*, 014304.
[15] E. J. Taffet, Y. Olivier, F. Lam, D. Beljonne, G. D. Scholes, *J. Phys. Chem. Lett.* **2018**, *9*, 1620.
[16] J. Föller, C. M. Marian, *J. Phys. Chem. Lett.* **2017**, *8*, 5643.
[17] R. Hamze, J. L. Peltier, D. Sylvinson, M. Jung, J. Cardenas, R. Haiges, M. Soleilhavoup, R. Jazzar, P. I. Djurovich, G. Bertrand, *Science* **2019**, *363*, 601.
[18] M. Gernert, L. Balles-Wolf, F. Kerner, U. Müller, A. Schmiedel, M. Holzapfel, C. M. Marian, J. Pflaum, C. Lambert, A. Steffen, *J. Am. Chem. Soc.* **2020**, *142*, 8897.
[19] R. Hamze, S. Shi, S. C. Kapper, D. S. Muthiah Ravinson, L. Estergreen, M.-C. Jung, A. C. Tadle, R. Haiges, P. I. Djurovich, J. L. Peltier, *J. Am. Chem. Soc.* **2019**, *141*, 8616.
[20] A. S. Romanov, L. Yang, S. T. Jones, D. Di, O. J. Morley, B. H. Drummond, A. P. Reponen, M. Linnolahti, D. Credgington, M. Bochmann, *Chem. Mater.* **2019**, *31*, 3613.
[21] F. Chotard, A. S. Romanov, D. L. Hughes, M. Linnolahti, M. Bochmann, *Eur. J. Inorg. Chem.* **2019**, *2019*, 4234.
[22] A. S. Romanov, S. T. Jones, L. Yang, P. J. Conaghan, D. Di, M. Linnolahti, D. Credgington, M. Bochmann, *Adv. Opt. Mater.* **2018**, *6*, 1801347.
[23] P. J. Conaghan, S. M. Menke, A. S. Romanov, S. T. Jones, A. J. Pearson, E. W. Evans, M. Bochmann, N. C. Greenham, D. Credgington, *Adv. Mater.* **2018**, *30*, 1802285.
[24] A. S. Romanov, C. R. Becker, C. E. James, D. Di, D. Credgington, M. Linnolahti, M. Bochmann, *Chemistry* **2017**, *23*, 4625.
[25] A. S. Romanov, M. Bochmann, *J. Organomet. Chem.* **2017**, *847*, 114.
[26] A. S. Romanov, D. Di, L. Yang, J. Fernandez-Cestau, C. R. Becker, C. E. James, B. Zhu, M. Linnolahti, D. Credgington, M. Bochmann, *Chem. Commun.* **2016**, *52*, 6379.
[27] H. H. Cho, A. S. Romanov, M. Bochmann, N. C. Greenham, D. Credgington, *Adv. Opt. Mater.* **2021**, *9*, 2001965.
[28] X. Ai, E. W. Evans, S. Dong, A. J. Gillett, H. Guo, Y. Chen, T. J. Hele, R. H. Friend, F. Li, *Nature* **2018**, *563*, 536.
[29] A. Abdurahman, T. J. Hele, Q. Gu, J. Zhang, Q. Peng, M. Zhang, R. H. Friend, F. Li, E. W. Evans, *Nat. Mater.* **2020**, *19*, 1224.
[30] J. Sworakowski, J. Lipiński, K. Janus, *Org. Electron.* **2016**, *33*, 300.
[31] D. Di, A. S. Romanov, L. Yang, J. M. Richter, J. P. Rivett, S. Jones, T. H. Thomas, M. Abdi Jalebi, R. H. Friend, M. Linnolahti, *Science* **2017**, *356*, 159.
[32] H. Guo, Q. Peng, X.-K. Chen, Q. Gu, S. Dong, E. W. Evans, A. J. Gillett, X. Ai, M. Zhang, D. Credgington, *Nat. Mater.* **2019**, *18*, 977.
[33] J. W. Kim, S. I. You, N. H. Kim, J.-A. Yoon, K. W. Cheah, F. R. Zhu, W. Y. Kim, *Sci. Rep.* **2014**, *4*, 7009.
[34] O. V. Mikhnenko, P. W. Blom, T.-Q. Nguyen, *Energy Environ. Sci.* **2015**, *8*, 1867.
[35] J.-S. Huang, T. Goh, X. Li, M. Y. Sfeir, E. A. Bielinski, S. Tomasulo, M. L. Lee, N. Hazari, A. D. Taylor, *Nat. Photonics* **2013**, *7*, 479.
[36] W. A. Luhman, R. J. Holmes, *Adv. Funct. Mater.* **2011**, *21*, 764.
[37] H.-F. Xiang, Z.-X. Xu, V. Roy, C.-M. Che, P. Lai, *Rev. Sci. Instrum.* **2007**, *78*, 034104.
[38] Y. Kawamura, J. Brooks, J. J. Brown, H. Sasabe, C. Adachi, *Phys. Rev. Lett.* **2006**, *96*, 017404.
[39] G. D. Scholes, *Annu. Rev. Phys. Chem.* **2003**, *54*, 57.
[40] G. Ramos-Ortiz, Y. Oki, B. Domercq, B. Kippelen, *Phys. Chem. Chem. Phys.* **2002**, *4*, 4109.
[41] L. S. Devi, M. K. Al-Suti, C. Dosche, M. S. Khan, R. H. Friend, A. Köhler, *Phys. Rev. B* **2008**, *78*, 045210.
[42] H. Fukagawa, T. Shimizu, Y. Iwasaki, T. Yamamoto, *Sci. Rep.* **2017**, *7*, 1735.
[43] W. S. Jeon, T. J. Park, S. Y. Kim, R. Pode, J. Jang, J. H. Kwon, *Org. Electron.* **2009**, *10*, 240.
[44] S. M. Menke, R. J. Holmes, *J. Phys. Chem. C* **2016**, *120*, 8502.
[45] D. S. M. Ravinson, M. E. Thompson, *Mater. Horiz.* **2020**, *7*, 1210.
[46] H. Ye, D. H. Kim, X. Chen, A. S. Sandanayaka, J. U. Kim, E. Zaborova, G. Canard, Y. Tsuchiya, E. Y. Choi, J. W. Wu, *Chem. Mater.* **2018**, *30*, 6702.
[47] D.-H. Kim, A. D'aléo, X.-K. Chen, A. D. Sandanayaka, D. Yao, L. Zhao, T. Komino, E. Zaborova, G. Canard, Y. Tsuchiya, *Nat. Photonics* **2018**, *12*, 98.
[48] Z. Cui, S. Ye, L. Wang, H. Guo, A. Obolda, S. Dong, Y. Chen, X. Ai, A. Abdurahman, M. Zhang, *J. Phys. Chem. Lett.* **2018**, *9*, 6644.
[49] M. Tanaka, R. Nagata, H. Nakanotani, C. Adachi, *Commun. Mater.* **2020**, *1*, 18.
[50] T. Basel, D. Sun, B. Gautam, Z. V. Vardeny, *J. Lumin.* **2014**, *155*, 89.
[51] Q. Peng, P. Chen, F. Li, *Synth. Met.* **2013**, *173*, 31.
[52] C. Gärditz, A. G. Mückl, M. Cölle, *J. Appl. Phys.* **2005**, *98*, 104507.
[53] J. Xu, X. Tang, J. Deng, R. Pan, F. Qu, X. Zhao, Z. Xiong, *Chin. Sci. Bull.* **2019**, *64*, 694.
[54] Q. Peng, N. Gao, W. Li, P. Chen, F. Li, Y. Ma, *Appl. Phys. Lett.* **2013**, *102*, 88.
[55] J. E. Lawrence, A. M. Lewis, D. E. Manolopoulos, P. Hore, *J. Chem. Phys.* **2016**, *144*, 214109.
[56] C. S. B. Matthews, A. S. Romanov, N. C. Greenham, *J. Mater. Chem. C* **2022**, *10*, 14180.